Plasmon-enhanced Electron Harvesting in Robust Titanium Nitride Nanostructures

Brock Doiron[A*], Yi Li[D], Andrei Mihai[B], Ryan Bower[B], Neil McN. Alford[B], Peter K. Petrov[B], Stefan A. Maier[D,A], Rupert F. Oulton[A*]

[A] Department of Physics, Imperial College London, London, UK
[B] Department of Materials, Imperial College London, London, UK
[D] Nanoinstitut München, Fakultät für Physik, Ludwig-Maximilians Universität München, München, Germany
[*] Corresponding Authors

Abstract

Titanium nitride (TiN) continues to prove itself as an inexpensive, robust, and efficient alternative to gold in plasmonic applications. Notably, TiN has improved hot electron harvesting and photocatalytic abilities compared to gold systems, which we recently attributed to the role of oxygen in TiN and its native semiconducting TiO_{2-x} surface layer. Here, we explore the role of localized surface plasmon resonances (LSPRs) on electron harvesting across the TiN/TiO_{2-x} interface and probe the resilience of TiN nanoparticles under high-power laser illumination. To investigate this, we fabricate titanium nitride strips where the lateral confinement allows for polarization-selective excitation of the LSPR. Using ultrafast pump-probe spectroscopy, optical characterization and Raman vibrational spectroscopy we relate differences and changes observed in the electron behaviour to specific material properties. We observe plasmon-enhanced electron harvesting beyond what is expected resulting from the enhanced absorption of the plasmonic mode. We accredit this to the surface oxide damping the plasmon resonance providing additional nonradiative loss channels. Subsequently, we show that low-power annealing of the surface oxide layer reduces the trap density at the interface and increases the initial harvested electron concentration. The unique properties of TiN make it important in the future development of plasmonic electron harvesting applications.

Introduction

Titanium nitride has proven to be a very promising optical material with similar characteristics to gold but with a higher melting temperature[1,2] and compatibility with complementary metal-oxide-semiconductor (CMOS) fabrication[3]. Moreover, its optical properties are easily tunable[4,5] providing additional flexibility not possible with the monatomic noble metals. With broad, tunable resonances across the near-infrared, it shows superior photocatalytic performance to an equivalent gold system both in colloidal form[6] and deposited on semiconductor rods[7], with advantages also for solar energy harvesting and photocatalysis. Perhaps the most exciting attribute of TiN is its semiconducting native oxide; our previous work[8] showed that electron harvesting into the omnipresent titania surface oxide layer could be effective (on the order of $10^{19}\ m^{-3}$ for modest pump powers). Our previous work[4] used systematic material characterisation (XPS, spectroscopic ellipsometry) to investigate the underlying film and surface oxide layer properties of the materials used in this work. Additional X-ray diffraction (XRD) data is included in the Supporting Information (Figure S6). Subsequently, ultrafast optical measurements of TiON thin films were used to identify the recombination processes at this metal-semiconductor interface, which allowed us to engineer and optimize electron harvesting. We showed that oxygen inclusion during deposition facilitated the formation of a low-defect electron collection interface enabling electrons and holes to be separated on nanosecond timescales.

In both TiON-TiO_2 and TiN-TiO_2 systems, photo-excited electrons in metals are initially excited into states well above the Fermi level but quickly thermalize with other electrons and phonons. This occurs within a few tens of femtoseconds[9,10] for electron-electron thermalization and typically several picoseconds[11] for electron-phonon thermalization. However, a Schottky barrier between a metal and a semiconductor prevents carrier thermalization in the metal by separating those carriers with sufficient energy to traverse it. Upon harvesting excited electrons or holes into the semiconductor, they remain for orders of magnitude longer compared to direct thermalization in the metal[12,13]. During this time, these electrons (holes) remain in the TiO_2 conduction (valence) band and can readily participate in chemical reactions[14,15] enhancing the natural photocatalytic abilities of TiO_2[16] or be harvested as a current[17-19]. As nanostructures of many conventional metals absorb strongly across the visible regime[20], there has been particular interest in using these structures in clean energy applications where solar energy is converted into chemical or electrical energy. As well, integration of the metal with a semiconductor allows detection of sub-band-gap photons. The broadband absorption and integration capabilities of TiN are thus highly desirable attributes. Neither of these can be achieved with conventional plasmonic metals (Au, Ag and Cu) due to their relatively sharp plasmon resonances[21] and tendency to diffuse into silicon at elevated temperatures.[22]

In this work we investigate the role of localized surface plasmon resonances (LSPR) of TiN nanostructures on the transfer of electrons across the TiN-TiO_{2-x} metal-semiconductor interface. Localized surface plasmons arise due to collective motions of electrons near metal-dielectric interfaces, which can be resonant in finite sized metallic nanostructures[23]. Nanostructured titanium nitride strips enable a polarization-selective LSPR excitation that allows us to compare resonant and film-like properties on a single sample, eliminating the contribution of any material variation. We use ultrafast pump-probe spectroscopy to investigate the electron injection and recombination dynamics. By comparing resonant and non-resonant pumping we observe a dramatic increase in electron harvesting that cannot be explained by increased LSPR absorption alone. We postulate that the presence of the encapsulating surface oxide damps the plasmon resonance and introduces additional loss channels. This increases the overall absorption, which is supported by finite difference time domain (FDTD) simulations. Finally, we examine the resilience of our fabricated particles to high laser power intensities and observe an irreversible change to the electron dynamics at a relatively low power. Remarkably, this change which enhances the efficiency of electron harvesting, is not a result of the melting and deformation of the particle. Raman spectroscopy attributes these changes to the localized laser-annealing of the amorphous surface TiO_{2-x} layer into a more uniform, low-defect anatase form. This ordering of the crystal structure is likely to improve the overall photocatalytic performance as has been observed previously in literature. Titanium nitride's unique physical, electronic and optical properties make it a promising platform for plasmon-enhanced solar energy conversion for inexpensive and robust clean energy applications.

Methods

To examine the plasmonic behaviour of titanium nitride, strips (200 nm x 30 μm) were fabricated using a Cr-mask lift-off procedure on a fused quartz substrate. A negative-tone resist mask was patterned using electron beam lithography (Raith eLine), which is followed by evaporation of a Cr layer (95 nm) and resist removal. A 50 nm TiN layer is then deposited using RF magnetron sputtering from a titanium target in a N_2/Ar (30% N_2) plasma at 600°C and subsequently immersed in Cr-etchant resulting in uniform strips of titanium oxynitride directly on the fused quartz substrate. Figure 1a shows a scanning electron microscope (SEM) image of the resultant strips. Due to the lateral confinement of the structure it can support a localized plasmon resonance when excited with a polarization perpendicular to the length of the strip. When excited with a parallel polarization, absorption should resemble the thin film absorption characteristics. Using a simple transmission configuration with a focused spot from a SuperK Compact supercontinuum laser we observe a polarization-selective plasmon resonance shown in Figure 1b. It exhibits a broadband plasmon resonance characteristic of nanostrucutred titanium nitride with over

55% of the incident light being extinguished at the resonance peak. Such a structure allows us to investigate electron dynamics with and without exciting a plasmon resonance on the same sample, which precludes the influence of material variation, which can have a profound effect on the properties of titanium nitride.[24,25]

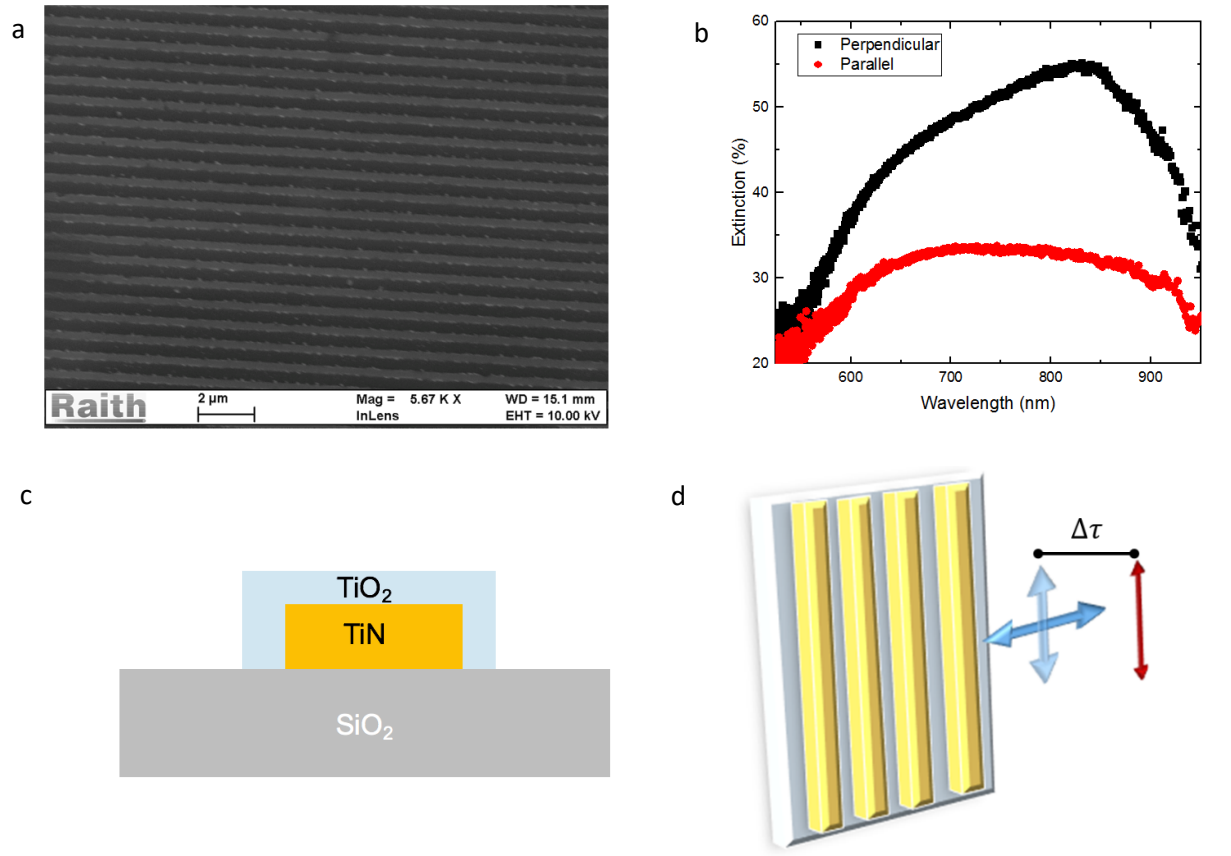

Figure 1 | Optical characterization of nanostructured titanium nitride strips. (a) Scanning electron microscope (SEM) image of the patterned titanium nitride strips on fused quartz coverslip using a Cr-liftoff procedure. The geometry of the strips (200 nm wide, 30 µm long) allows for polarization-selective excitation of the localized plasmon resonance (LSPR) resulting from the two-dimensional confinement of the metal. (b) Polarization-dependent transmission measurements of the strips using a SuperK Compact supercontinuum laser across the visible range. The enhanced absorption associated with exciting a plasmon resonance is clearly observed with a wavelength-dependent peak when exciting with a polarization perpendicular to the length of the strip. When exciting with a perpendicular polarization, absorption is lower and relatively flat across the measured range suggesting film-like absorption only. (c) Schematic of the physical system being measured including the fully-encompassing surface oxide layer. (d) Diagram showing the dense array of titanium nitride strips with a pump pulse (blue) and probe pulse (red) delayed by a time $\Delta\tau$ with respect to the pump. The arrows demonstrate the polarizations used during the experiment: the probe pulse is kept polarized along the length of the strip whereas the polarization of the pump is varied to study the role of surface plasmon decay on the electron collection into the surface TiO_{2-x} layer.

As shown in our previous work[8], the surface oxide (semiconducting TiO_{2-x}) plays a determining role in the electron dynamics as it can harvest the photoexcited electrons in the underlying TiN layer and delay recombination for nanoseconds timescales. Following the patterning process, a surface oxide forms on the sidewalls of the TiN strips in addition to the top surface as shown schematically in Figure 1c. Such a metal-semiconductor geometry will increase the electron harvesting efficiency as electrons can undergo multiple surface reflections.[26] In addition,

the initially excited electrons have momenta perpendicular to the side-wall surface (in line with the pump polarization) increasing the probability of harvesting the electrons[27,28]. To investigate the electron dynamics we use time-resolved pump-probe spectroscopy using two sub-200 femtosecond pulses generated from a Chameleon Ultra II Ti:Sapphire laser and an optical parametric oscillator (OPO). The pump pulse is of variable power (0.5-20 mW) across the wavelength range 790-860 nm and chopped mechanically. The time-delayed probe pulse is fixed at 1150 nm with a power of 150 μW and the differential reflection is detected using an InGaAs photodetector. We selectively excite the plasmon resonance by switching the polarization of the pump beam using a half-wave plate. The probe beam is kept parallel to the strips to exclude the influence of subsequent plasmonic effects, shown schematically in Figure 1d.

Results

The differential reflectivity is defined as the difference in reflected intensity of the probe with (I^{Pump}) and without (I^{NoPump}) the pump-induced excitation, normalized by the average reflected probe beam intensity collected at the detector:

$$\frac{\Delta R}{R} = \frac{I^{Pump} - I^{No\ Pump}}{\frac{1}{2}(I^{Pump} + I^{No\ Pump})}$$

For semiconductors this is directly proportional to the free carrier density[29] (N_{FC}). As we reported previously[8], the differential signature of titanium oxynitride is dominated by the excited electrons in the conduction band of the TiO_{2-x} semiconducting oxide layer. Thus, the differential reflectivity is a straightforward parameter for comparing electron harvesting efficiencies between samples and geometries. Firstly, we compare resonant and non-resonant excitation of the strips by changing the pump polarization to quantify the role of plasmon-enhanced hot electron generation on the overall harvesting efficiency (Figure 2a) excited with a 850 nm, 5 mW pump pulse. Indeed, the maximum measured differential reflectivity of the resonantly-excited sample is substantially higher than the non-resonant excitation. However, no difference in relaxation lifetimes is detected between the resonant and non-resonant excitation across the entire measured spectral range (780-860 nm) as shown in Supplementary Figure S5.

To verify this was not only a result of the more efficient absorption of the LSPR mode excited in the underlying TiN structure, we also present the differential reflectivity normalized by the measured extinction at 850 nm in Figure 2b. Higher absorption alone cannot explain the more efficient harvesting across the metal-semiconductor interface. In addition to having the side-walls as a collection surface perpendicular to the initial momentum of the electrons, the presence of the surface oxide will damp the plasmon resonance and provide

additional relaxation channels. This is brought about by the hybridization of modes of the two materials, similar to what occurs chemical interface damping[30,31]. However, care should be taken in this analogy as the hybridization of orbitals and conduction band states is a fundamentally different process. The additional loss channels increase the overall absorption of the structure and decrease the lifetime of the plasmon resonance. Using finite difference time domain (FDTD) simulations, we show the broadening and enhancement of the absorption cross section upon coating with TiO_2 (Supplementary Figure 1a). In Supplementary Figure 1b, we also show the simulated decay of the electric field at the surface of the particle as further evidence of the damping of the plasmon mode. In addition to the enhanced carrier harvesting observed upon resonant excitation, there are clearly observed oscillations of the measured differential reflectivity data present only when pumping on resonance. We attribute these oscillations to changes in absolute absorption due to thermally-induced lattice vibrations, or breathing modes.[32] The thermal expansion and contraction of the lattice, shifts the plasmon resonance resulting in a corresponding changes in absorption.

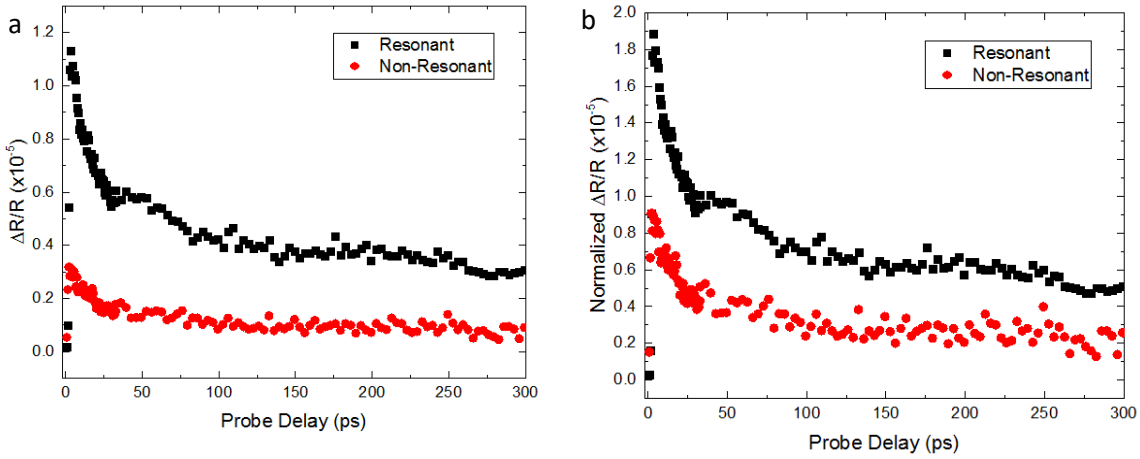

Figure 2 | Role of plasmon resonances on the electron transfer at the TiN-TiO_{2x} interface. Time-resolved differential reflectivity measurements for resonant (black) and non-resonant (red) excitation of the titanium nitride strips at 850 nm raw data (a) and normalized by the measured absorption of the strips (b). Even beyond the stronger absorption of the LSPR, there is more efficient electron harvesting upon resonant excitation. In addition to the interface being perpendicular to the initial momentum of the electrons, the presence of the surface oxide damps the plasmon resonance providing additional loss channels.

We investigated the resilience of the nanostructures by pumping on resonance with increasing power between 0.5 mW and 20 mW with a selection of the differential reflectivity signals shown in Figure 3a. Above 16 mW there is a dramatic change in the shape as seen in the bold blue and purple lines in Figure 3a, which stabilizes above 18 mW. This suggests a physical change of the system as the energy dissipation channels are altered resulting in more pronounced initial decay of the signal without a corresponding increase in maximum measured value. Following deliberate and sustained heating for 15 minutes at a laser power of 20 mW, measurements were

taken at decreasing laser powers. The measurements taken at lower powers then exhibit a distinctive and permanent change in the carrier dynamics, shown by the blue curve in Figure 3b, where the term "annealed" refers to the area exposed to the heating laser. The relative change in reflectivity of the annealed strips is enhanced up to 60% compared to the as-deposited measurement. Although the annealed sample has a larger number of initially harvested electrons, after 25 ps the as-deposited sample maintains the highest signal over the measured window. This can either be a result of an change in the density of traps (change in absolute value of free carriers) or change in carrier conduction away from the centre of the laser spot (change in average time of electron-trap collision). With TiO_{2-x} having a much lower melting temperature (1850 ˚C)[33] than titanium nitride (2930 ˚C)[34] it seems reasonable that the surface oxide will undergo changes before the underlying TiN, which will have a significant impact on the observed electron dynamics. This suggests that although TiN can maintain its properties under high power illumination, changes to the surface oxide occur well below the melting temperature of the nanostructure itself.

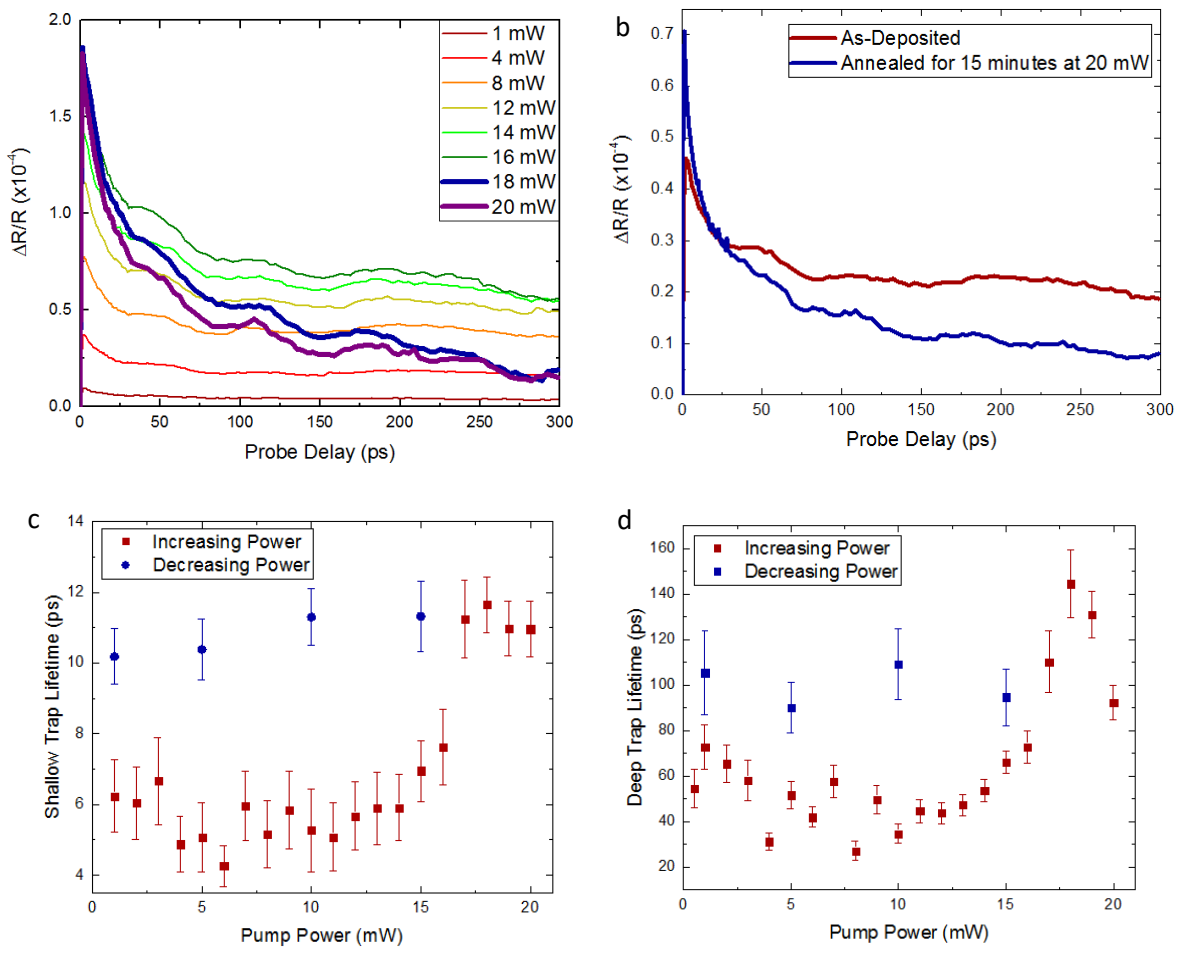

Figure 3 | High-power resilience measurements of titanium nitride strips and the associated electron dynamics. (a) Differential reflectivity traces with increasing power over the first 300 ps for resonant excitation. As power increases, the behaviour is seemingly unchanged until 14 mW where beyond this the signal saturates

and eventually degrades with a notable decrease in signal over the first 100 ps (blue and purple bolded curves). (b) Comparative plot of the differential reflectivity signal before and after the laser annealing process. (c-d) Shallow (c) and deep (d) trap lifetime fits according to electron kinetic model in Ref. 8 showing the permanent slowing of shallow trapping in the TiO_{2-x} layer. Red dots signify increasing laser power (low to high) and then blue dots represent measurements taken at decreasing laser power (high to low).

As a preliminary investigation of the laser-induced changes to the material, we fit the measured data to a bi-exponential electron kinetic model proposed in our previous work[8], which identifies the contribution of shallow and deep trap-mediated recombination. Details of the model are explained in Supplementary Section S2. In Figure 3c-d we plot the shallow trap lifetime (τ_{Sh}) and deep trap lifetime (τ_{DE}) associated with the rate of free electrons relaxing into oxygen vacancies in the TiO_{2-x} surface oxide layer. At higher laser powers we see a clear slowing (increase) of the shallow trap lifetime. In our previous work, we attributed these dynamics to less frequent trapping events and a decrease in oxygen vacancy density. We also see that upon decreasing the laser power (blue points in Figure 3c), it maintains this new post-anneal behaviour, indicating that it is a permanent change of the structure and not a non-linear phenomenon. Indeed, we do not observe a change in the morphology of the annealed strip as seen in scanning electron microscope imaging (Figure 4a) shown by the encircled regions. We thus hypothesise that the exposure to the high-power laser anneals the amorphous surface oxide to form a uniform anatase layer that provides a better contact with the underlying titanium nitride facilitating more efficient harvesting of electrons. From the literature, the amorphous to anatase transition is known to occur at relatively low temperatures (<400°C[35]) and the threshold is likely to be even lower for nanostructured TiO_2 with a thickness of several nanometres. However, from the brighter colour on SEM, the annealed surface oxide is determined to have lower conductivity, resulting in the less frequent trapping observed in Figure 3.

Upon such a reconfiguration of the lattice structure, there would be a distinctive change in the crystal vibrational modes resulting from ordering of the crystal planes. To probe the vibrational modes of the strips we illuminate the sample with a focused a green (532 nm) laser on a WiTEC Raman system. By collecting the scattered light we can construct a Raman spectrum of the sample, with peaks corresponding to vibrational modes of bonded atoms. Following exposure to high-intensity laser light for a length of time, the surface states of the film are modified locally as observed in the SEM image, herein referred to as an annealed area. By comparing the Raman spectra of an annealed and an unmodified area (Figure 4b), we observe a local change in the Raman spectrum of the exposed area. The key difference is the emergence of a new peak at 145 cm^{-1}, which is characteristic of anatase TiO_2 emerging after laser annealing.[36] This is consistent with our laser annealing hypothesis of the surface oxide layer.

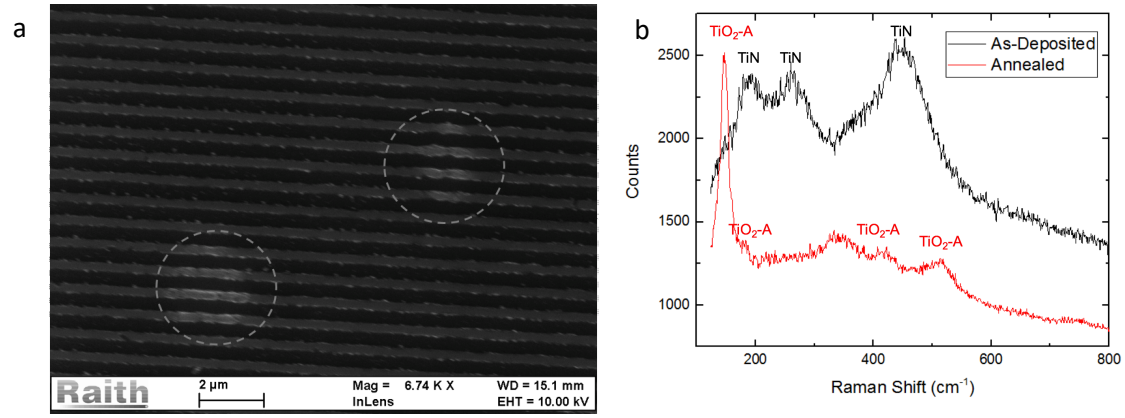

Figure 4 | Characterization of the titanium nitride strips following laser annealing. (a) Scanning electron microscope (SEM) imaging of the laser-annealed strips showing no deformation and thus the titanium nitride has not been melted. Dashed circles denote the areas annealed at 20 mW illumination for 15 minutes. (b) Raman vibrational spectroscopy of TiN before (black) and after laser annealing (red). Before annealing, there are no TiO_2 peaks suggesting the formation of an amorphous oxide layer as only the underlying TiON signal is observable. However, the annealed sample shows peaks distinctive of anatase TiO_2, which implies the laser annealing only annealed the surface oxide to be more ordered and have less oxygen vacancies as was suggested in Figure 3c.

Discussion

The potential influence of this laser annealing on the photocatalytic efficiency is not straightforward to determine from the differential reflectivity trace alone as it quantifies only the electron concentration in the surface oxide conduction band. A previous study of hybrid Au-TiO_2 superstructures[37] compared the photocatalytic ability of a conventional Au/TiO_2 aggregate nanoparticle system and one with Au particles on a TiO_2 mesocrystal. The key difference between the two is the ordered TiO_2 mesocrystal allows for the conduction of harvested electrons away from the Au and thus slowing recombination. This resulted in a much faster photocatalytic degradation of methyl blue under visible light irradiation and more efficient generation of H_2. Furthermore, conduction across the TiO_2 allows electrons to travel to traps resulting in a lower free carrier concatenation when full trap occupation is achieved. This is observed as a lower absolute value of the differential reflectivity (and in turn free carrier concentration) at 300 ps.

The dependence of the carrier concentration, as measured by the maximum differential reflectivity, on the plasmon resonance is shown in Figure 5a. Measurements are performed at 5 different pump wavelengths with the resonant behaviour reproduced in the perpendicular pump excitation. The parallel pump excitation (non-resonant) has a lower absolute value with no wavelength-dependence observed. The effectiveness of several different samples is summarized in Figure 5b, which shows the maximum carrier concentration for the film, non-resonant as-deposited, resonant as-deposited and resonant annealed strips. The large density of excited carriers in

the annealed sample suggests a high photocatalytic ability, immediately following pump excitation. However, to determine the explicit effect on photocatalysis, direct measurements will need to be completed on both isolated particles and strip geometry to determine the extent of electron conduction and its influence on photocatalytic ability.

a b

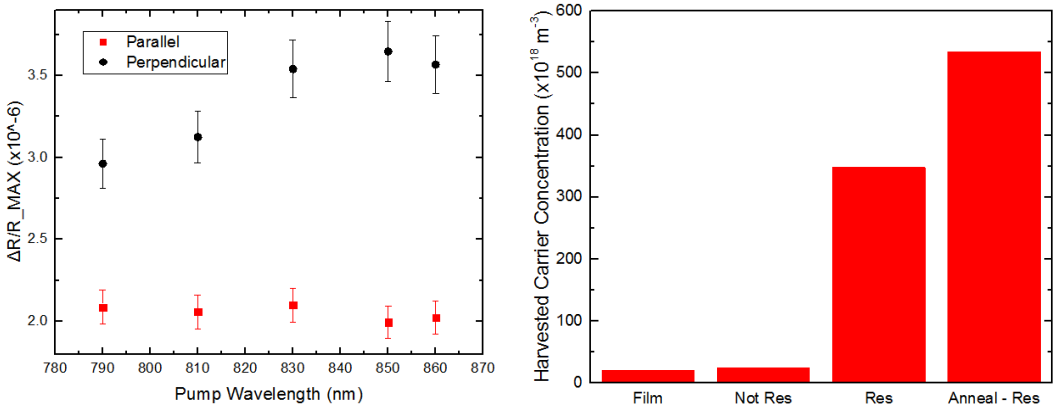

Figure 5 | Quantifying electron harvesting in titanium nitride. (a) Maximum differential reflectivity of the TiN strips measured with the two different pump polarisations. The resonant enhancement of the differential reflectivity, and in turn the harvested electron density, is clearly visible with the peak corresponding to the extinction peak in Figure 1b. (b) Estimates of the electron harvesting efficiency of a titanium nitride film and the titanium nitride strips measured at a pump power of 2 mW. Shown are the maximum harvested carrier concentration. As expected, the non-resonant excitation of the strips is similar to what is observed for the titanium nitride film. The role plasmon-enhanced electron harvesting is clear reaching well-over an order of magnitude higher concentrations in the annealed (20 mW laser illumination for 15 minutes) sample.

Conclusion

In this work, we explored the electron dynamics in nanostructured titanium nitride intended for use in photocatalytic applications. Carrier dynamics in TiN were affected by the unavoidable TiO_{2-x} surface layer, which delayed relaxation dependent on the availability of defects near the Ohmic metal-semiconductor interface. We used a strip geometry to easily compare the role of surface plasmon resonances and interface orientation on the harvesting of carriers excited in the TiN. We saw a clear enhancement of resonant excitation over non-resonant excitation of the strips beyond what is expected through the enhanced absorption. With support of finite difference time domain simulations, we established that this was a direct result of the surface oxide damping the resonance and providing additional loss channels at the metal-semiconductor interface. Using higher laser powers, we examined the resilience of the nanostructured titanium nitride and observe a distinctive behavioural change at relatively low powers. Following laser exposure, no melting or deformation of the particle was apparent, and so we looked to the surface oxide structure to explain the change in dynamics. Using Raman vibrational

spectroscopy, we detected a reconfiguration of the lattice structure of the surface oxide layer consistent with laser annealing from amorphous to anatase TiO_{2-x}. Using lifetime measurements of the electron recombination we confirmed that this process also reduced the density of oxygen vacancies, agreeing with the hypothesis of a more uniform, crystalline oxide layer, which allows for electron conduction away from the laser spot. This ability, along with a higher electron density collected following the decay of the plasmon, suggests that the annealed TiN may be favourable for electron harvesting and photocatalytic applications. The unique properties of titanium nitride and its ubiquitous surface oxide layer continues to prove its usefulness for electron harvesting applications and through careful examination of the material properties, an efficient, optimized and stable system can be achieved.

SUPPORTING INFORMATION

The supporting information in this work includes finite difference time domain (FDTD) data that investigates the role of the surface oxide in determining the properties of the surface plasmon resonance. As well, details of the trap-mediated relaxation model used to fit pump probe data is included. Pump-wavelength sweeps of the differential reflectivity magnitude and extracted lifetimes are presented for the entire wavelength range considered. Finally, X-ray diffraction data is presented for TiN showing details of the crystal structure.

ACKNOWLEDGEMENTS

We acknowledge support from the Engineering and Physical Sciences Research Council (EPSRC) Reactive Plasmonics Programme (EP/M013812/1), Lee-Lucas Chair in Physics, and the Henry Royce Institute made through EPSRC grant EP/R00661X/1.

CONTACT DETAILS

Brock Doiron (b.doiron15@imperial.ac.uk)

Rupert Oulton (r.oulton@imperial.ac.uk)

(1) Gui, L.; Bagheri, S.; Strohfeldt, N.; Hentschel, M.; Zgrabik, C. M.; Metzger, B.; Linnenbank, H.; Hu, E. L.; Giessen, H. Nonlinear Refractory Plasmonics with Titanium Nitride Nanoantennas. *Nano Lett.* **2016**, *16* (9), 5708–5713. https://doi.org/10.1021/acs.nanolett.6b02376.

(2) Guler, U.; Ndukaife, J. C.; Naik, G. V.; Nnanna, A. G. A.; Kildishev, A. V.; Shalaev, V. M.; Boltasseva, A. Local Heating with Lithographically Fabricated Plasmonic Titanium Nitride Nanoparticles. *Nano Lett.* **2013**, *13* (12), 6078–6083. https://doi.org/10.1021/nl4033457.

(3) Briggs, J. A.; Naik, G. V.; Petach, T. A.; Baum, B. K.; Goldhaber-Gordon, D.; Dionne, J. A. Fully CMOS-Compatible Titanium Nitride Nanoantennas. *Appl. Phys. Lett.* **2016**, *108* (5). https://doi.org/10.1063/1.4941413.

(4) Braic, L.; Vasilantonakis, N.; Mihai, A.; Villar Garcia, I. J.; Fearn, S.; Zou, B.; Alford, N. M. N.; Doiron, B.; Oulton, R. F.; Maier, S. A.; et al. Titanium Oxynitride Thin Films with Tunable Double Epsilon-Near-Zero Behavior for Nanophotonic Applications. *ACS Appl. Mater. Interfaces* **2017**, *9* (35), 29857–29862. https://doi.org/10.1021/acsami.7b07660.

(5) Liu, Y.; Kijima, S.; Sugimata, E.; Masahara, M.; Endo, K.; Matsukawa, T.; Ishii, K.; Sakamoto, K.; Sekigawa, T.; Yamauchi, H.; et al. Investigation of the TiN Gate Electrode with Tunable Work Function and Its Application for FinFET Fabrication. *IEEE Trans. Nanotechnol.* **2006**, *5* (6), 723–728. https://doi.org/10.1109/TNANO.2006.885035.

(6) Zheng, P.; Zhao, J.; Zheng, J.; Ma, G.; Zhu, Z. Non-Equilibrium Partial Oxidation of TiN Surface for Efficient Visible-Light-Driven Hydrogen Production. *J. Mater. Chem.* **2012**, *22* (24), 12116. https://doi.org/10.1039/c2jm30662j.

(7) Naldoni, A.; Guler, U.; Wang, Z.; Marelli, M.; Malara, F.; Meng, X.; Besteiro, L. V.; Govorov, A. O.; Kildishev, A. V.; Boltasseva, A.; et al. Broadband Hot-Electron Collection for Solar Water Splitting with Plasmonic Titanium Nitride. *Adv. Opt. Mater.* **2017**, *5* (15), 1601031. https://doi.org/10.1002/adom.201601031.

(8) Doiron, B.; Yi Li; Andrei Mihai; Stefano Dal Forno; Sarah Fearn; Lesley F Cohen; Neil M Alford; Johannes Lischner; Peter Petrov; Stefan A Maier; et al. Optimizing Hot Electron Harvesting at Planar Metal-Semiconductor Interfaces with Titanium Oxynitride Thin Films. *ArXiv* **2018**, 1–21.

(9) Voisin, C.; Christofilos, D.; Del Fatti, N.; Vallée, F.; Prével, B.; Cottancin, E.; Lermé, J.; Pellarin, M.; Broyer, M. Size-Dependent Electron-Electron Interactions in Metal Nanoparticles. *Phys. Rev. Lett.* **2000**, *85*, 2200–2203. https://doi.org/10.1103/PhysRevLett.85.2200.

(10) Watanabe, K.; Menzel, D.; Nilius, N.; Freund, H. J. Photochemistry on Metal Nanoparticles. *Chem. Rev.* **2006**, *106* (10), 4301–4320. https://doi.org/10.1021/cr050167g.

(11) Sun, C. K.; Vallée, F.; Acioli, L. H.; Ippen, E. P.; Fujimoto, J. G. Femtosecond-Tunable Measurement of Electron Thermalization in Gold. *Phys. Rev. B* **1994**, *50* (20), 15337–15348. https://doi.org/10.1103/PhysRevB.50.15337.

(12) Vickers, V. E. Model of Schottky Barrier Hot-Electron-Mode Photodetection. *Appl. Opt.* **1971**, *10* (9), 2190–2192. https://doi.org/10.1364/AO.10.002190.

(13) Lee, Y. K.; Jung, C. H.; Park, J.; Seo, H.; Somorjai, G. A.; Park, J. Y. Surface Plasmon-Driven Hot Electron Flow Probed with Metal-Semiconductor Nanodiodes. *Nano Lett.* **2011**, *11* (10), 4251–4255. https://doi.org/10.1021/nl2022459.

(14) Mubeen, S.; Lee, J.; Singh, N.; Krämer, S.; Stucky, G. D.; Moskovits, M. An Autonomous Photosynthetic Device in Which All Charge Carriers Derive from Surface Plasmons. *Nat. Nanotechnol.* **2013**, *8* (4), 247–251. https://doi.org/10.1038/nnano.2013.18.

(15) Bard, A. J.; Fox, M. A. Artificial Photosynthesis: Solar Splitting of Water to Hydrogen and Oxygen. *Acc. Chem. Res.* **1995**, *28* (3), 141–145. https://doi.org/10.1021/ar00051a007.

(16) Naldoni, A.; Altomare, M.; Zoppellaro, G.; Liu, N. Photocatalysis with Reduced TiO 2 : From Black TiO 2 to Cocatalyst- Free Hydrogen Production. **2019**. https://doi.org/10.1021/acscatal.8b04068.

(17) Li, W.; Valentine, J. G. Harvesting the Loss: Surface Plasmon-Based Hot Electron Photodetection. *Nanophotonics* **2017**, *6* (1), 177–191. https://doi.org/10.1515/nanoph-2015-0154.

(18) Knight, M. W.; Sobhani, H.; Nordlander, P.; Halas, N. J. Photodetection with Active Optical Antennas. *Science (80-.).* **2011**, *332* (6030), 702–704. https://doi.org/10.1126/science.1203056.

(19) McFarland, E. W.; Tang, J. A Photovoltaic Device Structure Based on Internal Electron Emission. *Nature* **2003**, *421* (6923), 616–618. https://doi.org/10.1038/nature01316.

(20) Link, S.; El-Sayed, M. A. M. Size and Temperature Dependence of the Plasmon Absorption of Colloidal Gold Nanoparticles. *J. Phys. Chem. B* **1999**, *103* (21), 4212–4217. https://doi.org/10.1021/jp984796o.

(21) Lalisse, A.; Tessier, G.; Plain, J.; Baffou, G. Quantifying the Efficiency of Plasmonic Materials for Near-Field Enhancement and Photothermal Conversion. *J. Phys. Chem. C* **2015**, *119* (45), 25518–25528. https://doi.org/10.1021/acs.jpcc.5b09294.

(22) Wilcox, W. R.; LaChapelle, T. J. Mechanism of Gold Diffusion into Silicon. *J. Appl. Phys.* **1964**, *35* (1), 240–246. https://doi.org/10.1063/1.1713077.

(23) Maier, S. A. *Plasmonics: Fundamanetals and Applications*; Springer Science & Business Media, 2007.

(24) Patsalas, P.; Kalfagiannis, N.; Kassavetis, S. Optical Properties and Plasmonic Performance of Titanium Nitride. *Materials (Basel).* **2015**, *8* (6), 3128–3154. https://doi.org/10.3390/ma8063128.

(25) Cuong, N. D.; Kim, D.-J.; Kang, B.-D.; Yoon, S.-G. Effects of Nitrogen Concentration on Structural and Electrical Properties of Titanium Nitride for Thin-Film Resistor Applications. *Electrochem. Solid-State Lett.* **2006**, *9* (9), G279. https://doi.org/10.1149/1.2216592.

(26) Blandre, E.; Jalas, D.; Petrov, A. Y.; Eich, M. Limit of Efficiency of Generation of Hot Electrons in Metals and Their Injection inside a Semiconductor Using a Semi-Classical Approach. *ACS Photonics* **2018**. https://doi.org/10.1021/acsphotonics.8b00473.

(27) Knight, M. W.; Wang, Y.; Urban, A. S.; Sobhani, A.; Zheng, B. Y.; Nordlander, P.; Halas, N. J. Embedding Plasmonic Nanostructure Diodes Enhances Hot Electron Emission. *Nano Lett.* **2013**, *13* (4), 1687–1692. https://doi.org/10.1021/nl400196z.

(28) Li, W.; Valentine, J. Metamaterial Perfect Absorber Based Hot Electron Photodetection. *Nano Lett.* **2014**, *14* (6), 3510–3514. https://doi.org/10.1021/nl501090w.

(29) Soltani, M.; Soref, R. Free-Carrier Electrorefraction and Electroabsorption in Wurtzite GaN. *Opt. Express* **2015**, *23* (19), 24984. https://doi.org/10.1364/OE.23.024984.

(30) Foerster, B.; Joplin, A.; Kaefer, K.; Celiksoy, S.; Link, S.; Sönnichsen, C. Chemical Interface Damping Depends on Electrons Reaching the Surface. *ACS Nano* **2017**, *11* (3), 2886–2893. https://doi.org/10.1021/acsnano.6b08010.

(31) Kale, M. J.; Christopher, P. Plasmons at the Interface. *Science (80-.).* **2015**, *349* (6248), 587–588. https://doi.org/10.1126/science.aac8522.

(32) Yi, C.; Su, M. N.; Dongare, P. D.; Chakraborty, D.; Cai, Y. Y.; Marolf, D. M.; Kress, R. N.; Ostovar, B.; Tauzin, L. J.; Wen, F.; et al. Polycrystallinity of Lithographically Fabricated Plasmonic Nanostructures Dominates Their Acoustic Vibrational Damping. *Nano Lett.* **2018**, *18* (6), 3494–3501. https://doi.org/10.1021/acs.nanolett.8b00559.

(33) O'Neil, M. J. *The Mereck Index - An Encyclopedia of Chemicals, Drugs, and Biologicals*; Royal Society of Chemistry: Cambridge, UK, 2013.

(34) Li, W.; Guler, U.; Kinsey, N.; Naik, G. V.; Boltasseva, A.; Guan, J.; Shalaev, V. M.; Kildishev, A. V. Refractory Plasmonics with Titanium Nitride: Broadband. *Adv. Mater.* **2014**, *26* (47), 7959–7965. https://doi.org/10.1002/adma.201401874.

(35) Khatim, O.; Amamra, M.; Chhor, K.; Bell, A. M. T.; Novikov, D.; Vrel, D.; Kanaev, A. Amorphous–Anatase Phase Transition in Single Immobilized TiO2 Nanoparticles. *Chem. Phys. Lett.* **2013**, *558*, 53–56. https://doi.org/10.1016/J.CPLETT.2012.12.019.

(36) Zhang, Q.; Ma, L.; Shao, M.; Huang, J.; Ding, M.; Deng, X.; Wei, X.; Xu, X. Anodic Oxidation Synthesis of One-Dimensional TiO 2 Nanostructures for Photocatalytic and Field Emission Properties. **2014**, *2014*.

(37) Bian, Z.; Tachikawa, T.; Zhang, P.; Fujitsuka, M.; Majima, T. Au/TiO2 Superstructure-Based Plasmonic Photocatalysts Exhibiting Efficient Charge Separation and Unprecedented Activity. *J. Am. Chem. Soc.* **2014**, *136* (1), 458–465. https://doi.org/10.1021/ja410994f.